

# 1 Statistical Properties of Electron Curtain Precipitation 2 Estimated with AeroCube-6

3 M. Shumko<sup>1,2</sup>, A.T. Johnson<sup>1</sup>, T.P. O'Brien<sup>3</sup>, D.L. Turner<sup>4</sup>, A.D. Greeley<sup>2</sup>,  
4 J.G. Sample<sup>1</sup>, J.B. Blake<sup>3</sup>, L.W. Blum<sup>2</sup>, A.J. Halford<sup>2</sup>

5 <sup>1</sup>Department of Physics, Montana State University, Bozeman, Montana, USA

6 <sup>2</sup>NASA's Goddard Space Flight Center, Greenbelt, Maryland, USA

7 <sup>3</sup>Space Science Applications Laboratory, The Aerospace Corporation, El Segundo, California USA

8 <sup>4</sup>Johns Hopkins Applied Physics Laboratory, Laurel, Maryland, USA

## 9 Key Points:

- 10 The dual AeroCube-6 CubeSats are used to identify stationary, narrow in latitude,  
11 and persistent > 30 keV precipitation termed curtains.
- 12 90% of the observed curtains in Low Earth Orbit are narrower than 20 kilome-  
13 ters in the latitudinal direction.
- 14 Some curtains were continuously accelerated into the atmosphere for multiple sec-  
15 onds.

Scattered?  
Precep.?

**Abstract**

Curtains are a recently discovered stationary, persistent, and latitudinally narrow electron precipitation phenomenon in low Earth orbit. Curtains are observed over consecutive passes of the dual AeroCube-6 CubeSats while their in-track lag varied from a fraction of a second to 65 seconds, with dosimeters that are sensitive to  $> 30$  keV electrons. This study uses the AeroCube-6 mission to quantify the statistical properties of 1,634 curtains observed over three years. We found that many curtains are narrower than 10 kilometers in the latitudinal direction with 90% narrower than 20 kilometers, corresponding to a few hundred kilometer radial size at the magnetic equator. We examined the magnetic local time and geomagnetic dependence of curtains. We found that curtains are observed in the late morning and midnight magnetic local times, with a higher occurrence rate at midnight, and curtains are observed more often during times of enhanced Auroral Electrojet. We found a few curtains in the bounce loss cone region above the north Atlantic, whose electrons were continuously scattered for at least 6 seconds as shown in one example. Such observations suggest that continuous curtain precipitation may be a significant loss of  $> 30$  keV electrons from the magnetosphere into the atmosphere, possibly scattered by a parallel direct current electric field.

**Plain Language Summary**

Electron curtain precipitation from space into Earth's atmosphere is a recently-discovered phenomenon observed by dual-spacecraft missions such as the AeroCube-6 CubeSats that orbit 700 kilometers above Earth's surface. Curtains appear stationary, remaining unchanged from seconds to a minute. Curtains are also very narrow along the satellite orbit that is mostly in the latitudinal direction. Besides these two properties, curtains and their impact on the magnetosphere and atmosphere are not well understood. Therefore, we used the AeroCube-6 mission that took data together for three years, to statistically quantify curtain properties and to better understand their origin. We found 1,634 curtains and found that 90% of curtains are narrower than 20 kilometers in the latitudinal direction, curtains are observed on the outer radiation belt field lines, and curtains are observed when the magnetosphere is disturbed. Curtains observed in a special region above the North Atlantic shed light on their origin. A few dozen curtains observed in this North Atlantic region were continuously precipitating into the atmosphere for multiple seconds, and are unlikely to be drifting. Therefore, curtains may be a significant source of atmospheric ionization responsible for the natural depletion of ozone.

**1 Introduction**

Energetic particle precipitation into Earth's atmosphere plays a fundamental role in controlling the dynamics of Earth's radiation belts, and ionization of Earth's upper atmosphere (e.g. Millan & Thorne, 2007; Randall et al., 2015). Even though particle precipitation, and its impact on the magnetosphere and the atmosphere, has been extensively studied since the 1960s, there are precipitation phenomena that are still poorly understood. One such form of precipitation that we have limited knowledge of are electron curtains.

Electron curtain precipitation is a stationary phenomenon observed in low Earth orbit (LEO). Curtains are narrow in latitude and persist for up to a minute between subsequent satellite passes. They were recently discovered by Blake and O'Brien (2016) using the  $> 30$  keV electron dosimeters onboard the dual AeroCube-6 (AC6) CubeSats that operated together between 2014 and 2017. This discovery was made possible by AC6's actively maintained in-track separation that varied between a few hundred meters and a few hundred kilometers. Besides the Blake and O'Brien (2016) study, not much is known about curtains including what they are, how are they generated, and their impact on the atmosphere. Answering these questions is an essential next step towards a more com-

66 plete understanding of how curtains, and particle precipitation in general, affect the mag-  
67 netosphere and Earth's atmosphere.

68 In low Earth orbit, curtains are narrower than a few tens of kilometers in the lat-  
69 itudinal direction. A polar-orbiting LEO satellite, such as AC6, will pass through the  
70 curtain cross-section in a few seconds, which appears in the electron count time series  
71 as short enhancements in flux. AC6 also observes similar-looking transient precipitation  
72 called electron microbursts. Curtains and microbursts are observed in the AC6 data but  
73 appear short-lived for different reasons: microbursts are temporal, while curtains are spa-  
74 tial. Hence AC6, and other recently developed multi-spacecraft missions, are necessary  
75 to identify and distinguish between transient microbursts and the persistent curtains.

76 Since the mid-1960s, microbursts have been observed by high altitude balloons where  
77 they appear as sharp peaks in flux with a sub-second duration (e.g. Anderson & Mil-  
78 ton, 1964; R. Brown et al., 1965; Parks, 1967). Because balloons are relatively station-  
79 ary, a microburst is easily classified as a transient phenomenon. Microburst electrons have  
80 also been directly observed by LEO satellites such as The Solar Anomalous and Mag-  
81 netospheric Particle Explorer (e.g. Blake et al., 1996; Lorentzen, Blake, et al., 2001; O'Brien  
82 et al., 2003; Douma et al., 2017). But a flux enhancement that looks like a microburst  
83 from a single LEO satellite is ambiguous—it can be transient or ~~persistent~~  
84 stationary and narrow in latitude. Thus, multi-spacecraft missions such as the Focused Investiga-  
85 tions of Relativistic Electron Burst Intensity, Range, and Dynamics (FIREBIRD-II) (Crew et al.,  
86 2016; Johnson et al., 2020) and AC6 (Blake & O'Brien, 2016; O'Brien et al., 2016) are  
87 necessary to resolve the temporal vs. spatial ambiguity. While this study focuses on cur-  
88 tain precipitation, microburst precipitation observed by AC6 was studied in Shumko et  
89 al. (2020).

90 While the impact of curtains on the magnetosphere and Earth's atmosphere is un-  
91 known, the impact of microbursts has been estimated to be substantial. Lorentzen, Looper,  
92 and Blake (2001), Thorne et al. (2005), Breneman et al. (2017), and Douma et al. (2019),  
93 among others, estimated that microbursts could deplete the outer radiation belt elec-  
94 trons in about a day. Furthermore, Seppälä et al. (2018) modeled a 6-hour microburst  
95 storm and concluded that microbursts depleted mesospheric ozone by roughly 10%. Mi-  
96 crobursts and curtains can be easily misidentified from a single satellite; if curtains are  
97 numerous, then the atmospheric and magnetospheric impact associated with microburst  
98 observations from single satellites may be overestimated.

99 Blake and O'Brien (2016) proposed a hypothesis that curtains are drifting remnants  
100 of microbursts. If a microburst is not completely lost in the atmosphere after the ini-  
101 tial scatter, the remaining microburst electrons will spread out (bounce phase disperse)  
102 along the entire magnetic field line over a few bounce periods. Concurrently these elec-  
103 trons drift to the east, with higher energy electrons drifting at a faster rate. Assuming  
104 this hypothesis, the initially localized microburst is also spread out in longitude into the  
105 shape of a curtain. A similar phenomena was hypothesized by Lehtinen et al. (2000) who  
106 predicted that drifting curtains can be created by energetic runaway beams driven by  
107 lightning, but these curtains ~~would~~ will be observed at relatively low L shells.

108 Precipitation bands, sometimes also referred to as spikes (e.g. Imhof et al., 1991),  
109 are another form of precipitation that ~~could~~ can be related to curtains. Precipitation bands  
110 are stationary and were observed to persist from an hour to as much as half a day (e.g.  
111 J. Brown & Stone, 1972; Blake et al., 1996). Blum et al. (2013) identified two precip-  
112 itation bands and estimated that only 20 precipitation bands can deplete all of the outer  
113 radiation belt electrons. The mechanism responsible for scattering precipitation band  
114 electrons at high L is believed to be field line curvature scattering, but the scattering mech-  
115 anism for band electrons at lower L shells is unknown. A few proposed scattering mech-  
116 anisms include wave-particle interactions and acceleration due to parallel direct current  
117 potentials (Hoffman & Evans, 1968).

This study expands on Blake and O'Brien (2016) by examining the statistical properties of curtains. We use 1634 confirmed curtain observations to study the distributions of the curtain: width in latitude, the geomagnetic conditions favorable to curtains, and the curtain distribution in L and magnetic local time (MLT). Lastly we will show examples of curtains that continuously precipitated in the bounce loss cone (BLC) region.

## 2 Instrumentation

The AC6 mission was a pair of 0.5U (10x10x5 cm) CubeSats built by The Aerospace Corporation and designed to measure the electron and proton environment in low Earth orbit (O'Brien et al., 2016). AC6 was launched on 19 June 2014 into a 620x700 km, 98° inclination orbit. The AC6 orbit over the three year mission lifetime was roughly dawn-dusk, and precessed only a few hours in MLT: 8-12 MLT in the dawn and 20-24 MLT in the dusk sectors. The two AC6 spacecraft, designated as AC6-A and AC6-B, separated after launch and were in proximity for the duration of the three-year mission—maintained by an active attitude control system. The attitude control system allowed them to actively control the amount of atmospheric drag experienced by each AC6 unit using the surface area of their solar panel “wings.” By changing their orientation, AC6 was able to maintain a separation between 2-800 km, confirmed by the Global Positioning System. The two AC6 units were in a string of pearls configuration, so one unit, typically unit A, was leading the other by an in-track lag: the time it would take the following spacecraft to catch up to the position of the leading spacecraft. To convert between the AC6 in-track separation and in-track lag, the AC6 orbital velocity was used. AC6’s orbital velocity was 7.6 km/s and varied by as much as 0.1 km/s. The in-track lag is readily available in the data files with the Global Positioning System, which makes it possible to remove the spatiotemporal ambiguity that affects single-spacecraft measurements.

Each AC6 unit contains three Aerospace microdosimeters (licensed to Teledyne Microelectronics, Inc) that measure the electron and proton dose in orbit (O'Brien et al., 2016). The dosimeter used for this study is dos1 with a  $> 30$  keV integral electron response, as the other dosimeters either responded primarily to protons or were not identical between unit A and B. All dosimeters sample at 1 Hz in survey mode, and 10 Hz in burst mode. 10 Hz data was readily available from both AC6 units from June 2014 to May 2017 while their in-track lag was less than 65 seconds. Figure A1 in the appendix shows the distribution of 10 Hz data as a function of AC6 in-track lag.

## 3 Methodology

### 3.1 Curtain Identification

The 10 Hz data were used to identify curtains using the following two criteria: a high spatial correlation, and a prominent peak. Before we applied the identification criteria, the AC6-B time series was shifted by the in-track lag to spatially align it with the AC6-A time series.

The first identification criterion is a 1-second rolling Pearson correlation applied to both time series. Spatial features with a correlation greater than 0.8 are considered highly correlated. The second criterion is applied to the highly correlated features to check if they are also prominently peaked. To find peaked precipitation, we used a similar technique to the technique used by Blum et al. (2015) to identify precipitation bands, and by Greeley et al. (2019) to identify microbursts. Our technique quantified the number of Poisson standard deviations,  $\sigma$ , that dos1 counts in each 100 ms bin are above a 10-second centered running average,  $b_{10}$ . Locations where dos1 counts are at least two  $\sigma$  above  $b_{10}$ , in other words  $dos1 > 2\sqrt{b_{10}} + b_{10}$ , are considered prominently peaked. One bias inherent to this detection algorithm, and similar algorithms such as the burst parameter (O'Brien et al., 2003), is a reduced sensitivity for wider peaks. For curtains with

*writing portions of time?*

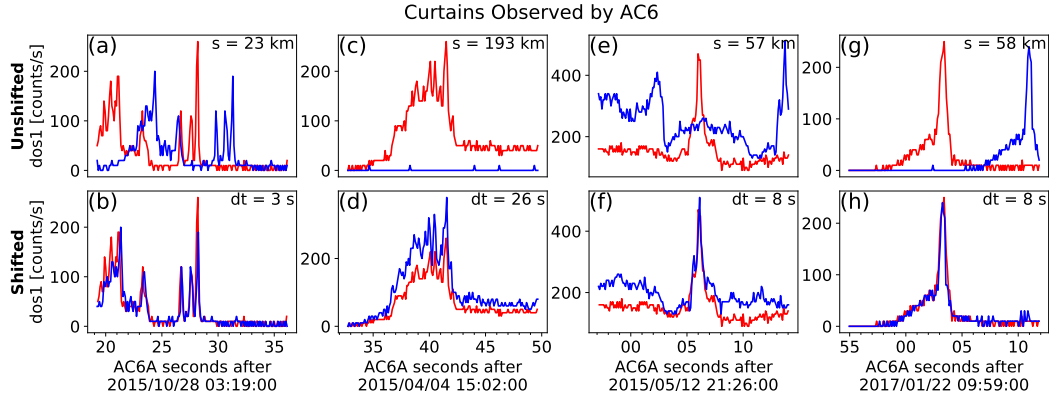


**Figure 1.** Four examples showing the  $> 30$  keV electron time series data taken by AC6 at the same time (unshifted) in the top row and at the same position (shifted by  $dt$  seconds) in the bottom row. AC6-A, whose data is shown with the red curves, was  $s$  kilometers ahead of AC6-B. To show the data at the same position the AC6-B time series was shifted by the in-track lag annotated by  $dt$ . These examples show that curtain precipitation was highly correlated for up to 26 seconds.

a width similar to  $b_{10}$ , the baseline will be significantly elevated making the curtain peak less pronounced.

We tuned the automated detection parameters to identify a large number of curtains. Once curtains were automatically identified, one author visually inspected 6,149 candidate curtains and verified 1,634 curtains. The visual inspection was performed to remove ambiguous detections where the peaks lined up in space and time, and false positive detections that were triggered by three conditions: sharp count rate shoulders, low baseline ( $b_{10}$ ), and high correlations resulting from Poisson noise. Four curtain examples are shown in Fig. 1. In each instance, the unmodified time series is shown in the top row and the spatially-aligned time series in the bottom row. The in-track lag used to shift the bottom row is annotated by  $dt$ , corresponding to an AC6 in-track separation annotated by  $s$ . The bottom row shows highly correlated curtains observed at the same location for at least 3 to 26 seconds.

### 3.2 Differentiating Between Drifting and Precipitating Curtains

The AC6 dosimeters lack the necessary pitch angle resolution to differentiate between locally drifting and precipitating electrons to test the Blake and O'Brien (2016) hypothesis that curtains are the drifting remnants of microbursts. Fortunately, one standard method of distinguishing between locally precipitating, drifting, and trapped particles is by using the geographic location of observations with respect to the location of the South Atlantic Anomaly (SAA).

Earth's magnetic field is asymmetric and has a region of weaker magnetic field in the South Atlantic Ocean called the South Atlantic Anomaly. The weaker magnetic field in the SAA naturally differentiates particles by pitch angle into trapped and quasi-trapped populations. While some particles observed in LEO are trapped and will execute closed drift paths, most particles observed in LEO are quasi-trapped: they drift around the Earth until they reach the SAA. Within the SAA, the weaker magnetic field strength can lower the particle's mirror point altitude into the atmosphere, where collisions with the atmospheric neutrals and ions are more numerous and the particle is lost.

195 Particles that are quasi-trapped have pitch angles in the drift loss cone and will pre-  
 196 precipitate within one drift period (often within the SAA) (e.g. Selesnick et al., 2003). Part-  
 197 ticles with smaller equatorial pitch angles that are lost in the atmosphere within one bounce  
 198 are in the bounce loss cone (BLC). Traditionally, a particle is in the BLC if its mirror  
 199 point altitude is at or below 100 km in either hemisphere (e.g. Selesnick et al., 2003). *(ok just ref.  
here (thin))*

200 In most regions outside of the SAA and its conjugate point in the North Atlantic,  
 201 AC6 will observe a combination of drift and bounce loss cone electrons. In the SAA, AC6  
 202 does not only observe electrons that are immediately lost, but a combination of electrons  
 203 that are in the drift loss cone, bounce loss cone, and trapped (a trapped electron that  
 204 locally mirrors at AC6's altitude in the SAA will mirror at higher altitudes everywhere  
 205 else). In the region magnetically conjugate to the SAA in the North Atlantic, AC6 only  
 206 observes electrons in the BLC. ~~Here, if an electron makes it to AC6's altitude, it might~~  
 207 ~~be in the local loss cone and precipitate in the local hemisphere. Alternatively, the elec-~~  
 208 ~~tron may mirror at or below AC6 and bounce to its conjugate mirror point deep in the~~  
 209 ~~atmosphere or below sea level in the SAA.~~ Therefore, any electrons observed in the BLC  
 210 region will likely precipitate within one bounce ( $\approx 1.5$  seconds for 30 keV electrons).

211 We estimated the BLC region for locally-mirroring electrons in the North Atlantic  
 212 Ocean using the IRBEM-Lib magnetic field library and the Olson-Pfizer magnetic field  
 213 model (Boscher et al., 2012; Olson & Pfizer, 1982). We defined a latitude-longitude grid,  
 214 with a  $\approx 0.5^\circ \times 0.5^\circ$  grid size, spanning the North Atlantic at 700-kilometers altitude,  
 215 and estimated the local magnetic field strength. The 700-kilometers altitude was cho-  
 216 sen because it is the upper bound altitude for AC6's orbit and it is the conservative limit  
 217 because at lower altitudes the BLC region is larger. For each latitude-longitude point  
 218 we traced the magnetic field line to the southern hemisphere and found the conjugate  
 219 mirror point altitude. If the conjugate mirror point is  $\leq 100$  kilometers, the electron is  
 220 likely lost and the associated grid point is in the BLC. Furthermore, a more rigorous bounce  
 221 loss cone criterion is the conjugate mirror point altitude below sea level. In this case, the  
 222 electron is ~~likely~~  
 223 lost. Since AC6 can measure locally-mirroring electrons in the North  
 224 Atlantic, the spacecraft altitude determines the upper bound conjugate mirror point al-  
 225 *? x*  
 226 titude in the SAA. The BLC region estimated by this method closely matches the BLC  
 227 region shown in Comess et al. (2013, Figure 1) and Dietrich et al. (2010, Figure 3) for  
 228 other LEO satellites. Furthermore, we repeated the same analysis using the Tsyganenko  
 229 1989 model (Tsyganenko, 1989), which yielded similar boundaries.

## 228 4 Results

229 In this study we addressed three questions: what is the distribution of curtain widths  
 230 along the AC6 orbit (mostly in geographic latitude), when and where are curtains ob-  
 231 served, and are curtains due to drifting or locally precipitating?

*composed of electrons*

### 232 4.1 Curtain Width

233 The curtain width is quantified as the width at half of the curtain's topographic  
 234 prominence ~~that is~~ described in Appendix B. The spatial width of a curtain is then the  
 235 product of the observed width in time and AC6's orbital velocity. The curtain width is  
 236 measured along AC6's orbit track which is mostly in the latitudinal direction, therefore  
 237 the estimated curtain widths are also mostly in the latitudinal direction. The distribu-  
 238 tion of curtain widths is shown in Fig. 2. Curtains are very narrow. Many curtains are  
 239 narrower than 10 km in the latitudinal direction, and 90% are narrower than 20 km.

### 240 4.2 When and Where Are Curtains Observed

241 The distribution of curtains in L and MLT is shown in Fig. 3. Figure 3a shows the  
 242 distribution of the observed curtains, while Fig. 3b shows the same distribution normal-

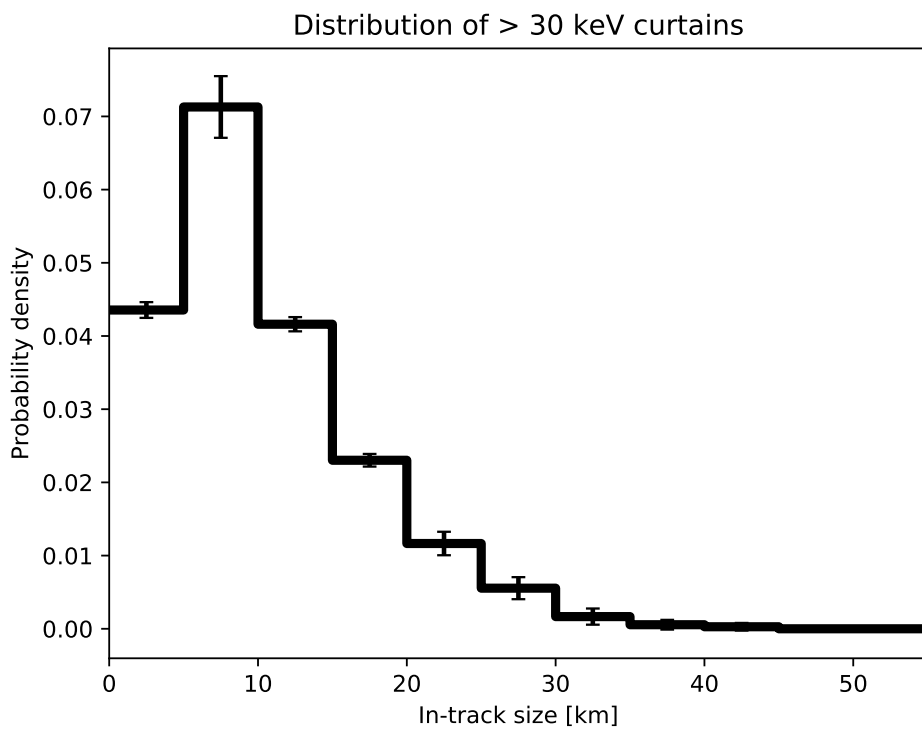


**Figure 2.** The distribution of curtain widths along the AC6 orbit that is mostly in the latitudinal direction. The error bars are derived assuming the Poisson standard error.

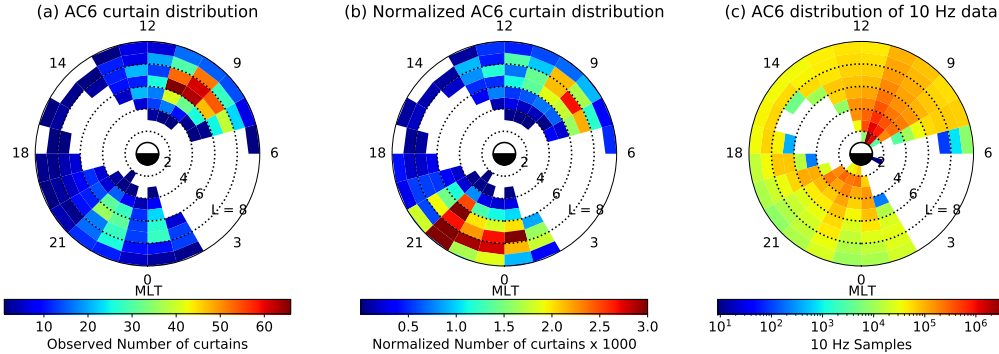


**Figure 3.** The distribution of observed curtains by L shell and MLT. Panel a shows the locations of all observed curtains used in this study. Panel b shows the curtain distribution normalized by the number of quality 10 Hz samples taken in each bin, shown in panel c. The white bins in panels a and b show where no curtains were observed. In panel c the white bins show where AC6 did not take any 10 Hz data at the same location.

243  
244  
245  
246  
247  
248  
249  
250  
251  
252  
253  
254  
255  
256  
257  
258  
ized by the number of quality 10 Hz samples (flag = 0 in the data files) that AC6 took  
at the same location in each L-MLT bin. In Fig. 3a and 3b, the bins with where no curtains were observed are white. The AC6 sampling distribution is shown in Fig. 3c, whose  
white bins show where AC6 did not take any 10 Hz data at the same location. The normalized curtain distribution in Fig. 3b shows an enhanced curtain occurrence in the outer radiation belt  
*(L ~ 5 - 8)*

We also examine the geomagnetic conditions favorable for curtains. Figure 4a shows the distribution of the minute cadence Auroral Electrojet (AE) index between 2014 and 2017 in solid black, for times when quality dos1 data were available from both AC6 units. Furthermore, the distribution of the AE index when curtains were observed is shown by the solid blue lines. Curtains are observed during both low and high geomagnetic activity, slightly more often at higher AE than the index itself (curtain distribution trends above the AE index when  $AE > 200$ ). Lastly, we normalized the curtain distribution in Fig. 4a assuming any AE index is equally probable. The normalized curtain distribution is shown in Fig. 4b, which emphasizes that the curtain occurrence frequency increases with increasing AE index.

#### 259 4.3 Local Atmospheric Precipitation

260  
261  
262  
263  
264  
265  
266  
267  
268  
Lastly we investigate if curtains are drifting or locally precipitating. Figure 5a shows a map of the northern BLC region in the North Atlantic. The solid blue line is the northern boundary where an electron that mirrors locally at 700 km has a conjugate mirror point at 100 km in the SAA. Immediately south of the solid blue line, the conjugate mirror altitude rapidly decreases towards, and below, sea level. The dashed blue line is the boundary where the conjugate mirror point altitude is at sea level. South of this line the conjugate mirror point is inside the Earth. For reference, AC6 takes about 30 seconds to move between the solid and dashed blue curves. The two dotted black curves in Fig. 5a are roughly the boundary of the outer radiation belt, defined as  $L = 4 - 8$ .

269  
270  
271  
Of the 1634 curtains, we found 36 curtains that were observed inside the BLC region. Figure 5b-e shows 4 curtain examples (AC6-B time shifted by the in-track lag), along with the AC6 in-track lag, L and MLT during the observations annotated. The

### The distribution of the Auroral Electrojet index for curtains

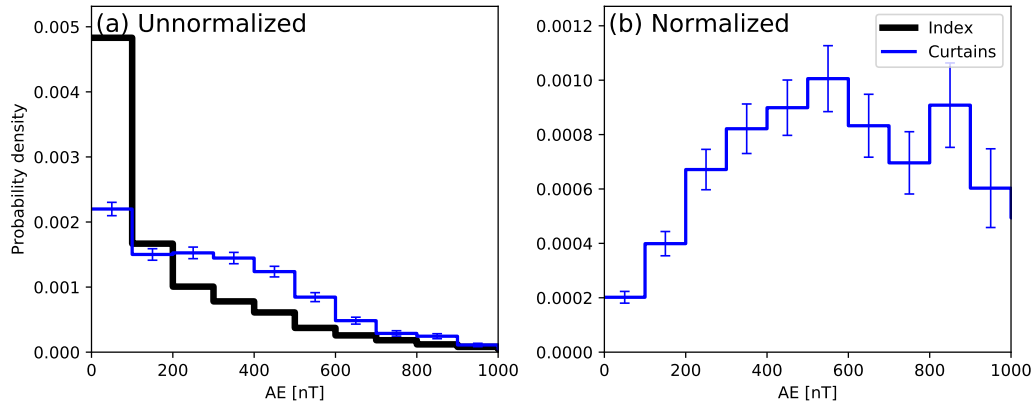


**Figure 4.** The distribution of the Auroral Electrojet (AE) index when curtains were observed. The blue line in panel a shows the distribution of AE when curtains where observed, and for reference the black line is shows the distribution of the entire AE index between 2014 and 2017 when quality 10 Hz data is available from both AC6 spacecraft. Panel b shows the curtain distribution normalized by the AE index distribution, and it represents the distribution assuming that any AE index is equally probable. The error bars are derived assuming the Poisson standard error.

AC6 locations where these curtains were observed are shown in Fig. 5a with the red stars and the corresponding panel labels.

## 5 Discussion

### 5.1 Curtain Width

Curtains are narrow in latitude. Figure 2 shows that the width of most curtains is on the order of 1–3 seconds in time as observed by AC6, corresponding to a 8–20 kilometer spatial width along the AC6 orbit track. Scaled to the magnetic equator, these widths correspond to a source with a radial scale size of a few hundred kilometers. The reduced sensitivity of the detection algorithm, as described in Section 3.1, is unlikely to significantly underestimate the curtain width distribution because most curtains had a width less than half of the 10-second baseline's width.

As shown in Fig. 1, it is remarkable that some curtains maintain a fine structure after multiple seconds with little observable difference. However, sometimes curtains appear to be slightly and systematically shifted in latitude, while maintaining their fine structure (not shown).

### 5.2 When and Where Are Curtains Observed

Figure 3b shows that curtains likely originate in the outer radiation belt and are observed relatively more in the pre-midnight than late-morning MLT regions. Furthermore, curtains are more often observed at higher L shells near midnight MLT; however the sampling statistics at high L are limited because AC6 rapidly crosses high L shells. Nevertheless, Fig. 3b hints that curtains near midnight MLT were observed at L shells possibly outside the outer radiation belt. Lastly, Figure 4b shows that curtains are associated with an enhanced AE.

...some comparison to distributions of other precipi phenomena?

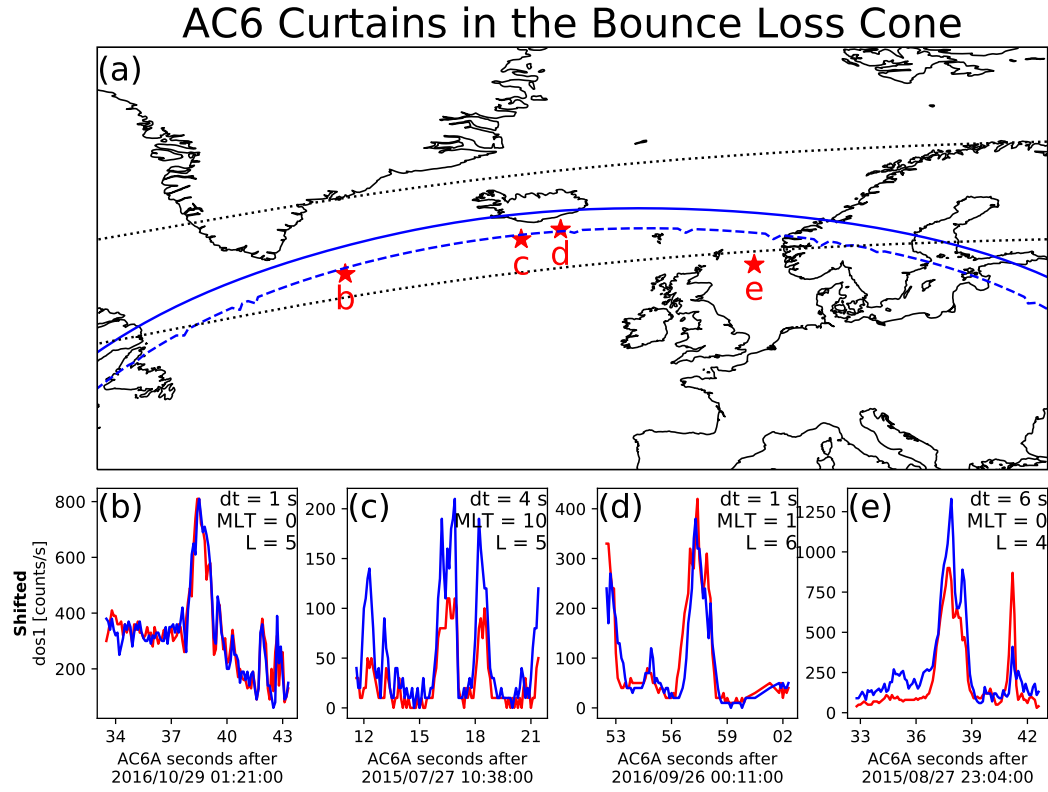


**Figure 5.** Curtains observed in the bounce loss cone region. Panel a shows a map of the North Atlantic region with the outer radiation belt, defined by  $L = 4 - 8$ , shown with the dotted black curves. The solid blue curve shows the northern boundary of the bounce loss cone region. Along this curve, electrons locally mirroring at 700 kilometers altitude have a conjugate mirror point at 100 kilometers altitude in the SAA. A more strict bounce loss cone criterion is the dashed blue curve that represents a conjugate mirror point altitude at sea level in the SAA. The 4 red stars with labels show the locations of the curtain examples shown in the corresponding panels b-e. The panels b-e show the 4 example curtains with the AC6-A data shown by the red line and the time-shifted AC6-B data with the blue line. The annotations in each example show the AC6 in-track lag ( $dt$ ),  $L$ , and MLT rounded to the nearest integer. AC6-A was leading in all examples except in panel d.

### 295      5.3 Curtains Observed in The Bounce Loss Cone

296      The handful of curtains observed in the bounce loss cone, and shown in Fig. 5, put  
 297      the Blake and O'Brien (2016) curtain drift hypothesis into question. These curtains were  
 298      observed near the sea level mirror altitude curve. One possible explanation is that the  
 299      drifting curtain electrons were observed at the end of their drift orbit, however because  
 300      these examples were seen far from the western edge of the BLC, any drifting electrons  
 301      would have been lost before AC6 observed them. Thus, they were not drifting and were  
 302      precipitating for as long as 6 seconds, as shown in Fig. 5e. The curtain precipitation per-  
 303      sisted for multiple bounce periods ( $\approx 1.5$  seconds for 30 keV electrons in this region).  
 304      There are relatively few mechanisms capable of persistently scattering electrons. The scat-  
 305      tering mechanism must be radially localized; if we assume the mechanism is at the mag-  
 306      netic equator, it must be on a scale of a few hundred kilometers.  
 307      One candidate mech-  
 308      anism is a direct current electric field that is parallel to the background magnetic field  
 309      that lowers the electron mirror point to AC6 altitudes. To find the minimum potential  
 310      we assume the electron is barely trapped and has a 100-kilometer conjugate mirror point  
 311      altitude in the SAA, so initially the electron will mirror above AC6 in the bounce loss  
 312      cone region.

312      To find the parallel potential,  $q\Phi$ , we use the kinetic energy,  $W$ , of a 30 keV elec-  
 313      tron at its initial mirror point with a magnetic field strength of  $B_i$ . The kinetic energy  
 314      at the initial mirror point can be written as  $W_i = \mu B_i$  where  $\mu$  is the first adiabatic  
 315      invariant that is conserved during this acceleration. When a parallel potential acceler-  
 316      ates the electron of charge  $q$  and does  $q\Phi$  amount of work, the electron will mirror closer  
 317      to Earth's surface and mirror at a field strength  $B_f$  where its final energy is  $W_f = \mu B_f$ .  
 318      Now we relate the initial and final kinetic energy of the electron,

$$312 \quad \mu B_f = \mu B_i + q\Phi. \quad (1)$$

319      Then we solve for  $q\Phi$  and substitute  $\mu$  to express the above equation as a function of the  
 320      initial kinetic energy

$$321 \quad q\Phi = W_i \frac{(B_f - B_i)}{B_i}. \quad (2)$$

322      The parallel potential is proportional to  $W_i$  so a larger potential is necessary to accel-  
 323      erate higher energy electrons. AC6 dos1 electron energy response increases rapidly from  
 324      30 keV to a peak at 100 keV (Figure 2 in O'Brien et al., 2019), therefore our assump-  
 325      tion that  $W_i = 30$  keV can underestimate the parallel potential. However, the counts  
 326      observed by AC6 are a convolution of, among other things, the AC6 dos1 electron en-  
 327      ergy response and the falling electron energy spectrum. Thus, the majority of electrons  
 328      that AC6 observed have energies close to 30 keV and the  $W_i = 30$  is an appropriate  
 329      approximation.

329      We again used IRBEM-Lib to estimate  $q\Phi$ . For each example curtain in Fig. 5, we  
 330      first estimated the local magnetic field,  $B_f$ , that the electron descended to after the ac-  
 331      celeration. Then we traced the local field line into the SAA. We estimated  $B_i$  at 100 kilo-  
 332      meters altitude in the SAA for barely trapped electrons. With the initial and final  $B$ ,  
 333      along with  $W = 30$  keV, the minimum potential was between  $q\Phi = 1 - 4$  kV for the  
 334      examples shown in Fig. 5.

335      The range of estimated potentials is typical for the inverted-V discrete aurora. Partamies  
 336      et al. (2008) used the observations made by the Fast Auroral SnapshoT (FAST) mission,  
 337      They reported that the auroral inverted-V electron precipitation structures, with elec-  
 338      tron energies up to a few tens of keV, were accelerated by 2-4 kV parallel potentials. The  
 339      inverted-V structure and curtains share several similarities including: latitudinal width,  
 340      high occurrence rate in the midnight MLT region, and the maximum inverted-V energy

*red handwritten notes:*  
 1. "no S. S. S." (near top left)  
 2. "This is?" (near middle left)  
 3. "suggested ans gen" (near top right)  
 4. "mech must be capable of persistently sat. e-s." (near middle right)

341 extends into tens of keV (e.g. Marklund et al., 2011; Thieman & Hoffman, 1985). AC6's  
 342 dos1, with its 30 keV electron threshold, may by observing the highest energy tip of the  
 343 inverted-V aurora. A possible connection between the inverted-V structures is intriguing,  
 344 but by itself AC6 cannot easily test this hypothesis. To investigate further, a follow-  
 345 on study could look at ground-based auroral imager data and look for meso-scale auro-  
 346 ral arcs when AC6 observed curtains overhead.

347 Regardless of the source of the curtain precipitation, the impact of curtains on the  
 348 atmosphere needs to be quantified. Even if the curtains observed in the BLC are the ex-  
 349 ception and other curtains are drifting, the drifting curtains will still precipitate within  
 350 one drift period. Precipitating electrons produce odd reactive nitrogen ( $\text{NO}_x$ ) molecules  
 351 that are currently underestimated by atmospheric models such as the widely-used Whole  
 352 Atmosphere Community Climate Model (WACCM) (e.g. Randall et al., 2015). Curtain  
 353 precipitation could explain the lack of atmospheric  $\text{NO}_x$ . However, an AC6-like mission  
 354 with pitch angle and energy resolution will be necessary to quantify the curtain impact  
 355 on the atmosphere.

## 356 6 Conclusions

357 The 1,634 curtains examined here allowed us to make the following inferences:

- 358 1. Curtains are narrow—90% are less than 20 kilometers wide in the latitudinal di-  
 359 rection.
- 360 2. Curtains are observed predominately in the pre-midnight MLT region, and dur-  
 361 ing active geomagnetic periods.
- 362 3. Some curtains continuously precipitate into the atmosphere for multiple seconds.

363 As shown in Fig. 1, curtain precipitation is narrow with a fine structure that per-  
 364 sists for multiple seconds: for at least 26 seconds as shown in Fig. 1d. Either the scat-  
 365 tering mechanism that continuously generates curtains is physically static for multiple  
 366 seconds, or the curtain electron drift is often undisturbed. ✓✓

367 The curtain-microburst relationship hypothesized in Blake and O'Brien (2016) is  
 368 not clear. Curtains observed in the bounce loss cone cast doubt on the curtain-microburst  
 369 hypothesis. Some curtains continuously precipitate for at least a few seconds, and can  
 370 be a significant source of energetic electron precipitation into the atmosphere. Lastly,  
 371 we found that the continuous scattering of curtain electrons can be explained by a par-  
 372 allel direct current electric field, possibly relating curtains to the aurora.

## 373 Appendix A Distribution of Colocated 10 Hz Data

374 Figure A1 shows the distribution of colocated AC6 10 Hz data as a function of in-  
 375 track lag. This distribution is heavily dominated by small in-track lags and 72% of the  
 376 colocated 10 Hz data was taken when AC6 was separated in-track by less than 10 sec-  
 377 onds, corresponding to 75 km in-track separation. Therefore, most of the curtains stud-  
 378 ied here were observed for small in-track lags, which limits our ability to explore the ex-  
 379 tent of curtain duration.

## 380 Appendix B Estimating Curtain Widths

381 The curtain width in the dos1 time series is defined here as the width at half of the  
 382 curtain's topographic prominence. Topographic prominence for a peak in a time series  
 383 is the height of a peak relative to the maximum of the two minima on either side of the  
 384 peak. The minima on either side of the peak are searched for between the peak and the  
 385 nearest higher peak on that side. Figure B1 shows 5 examples of curtains observed by

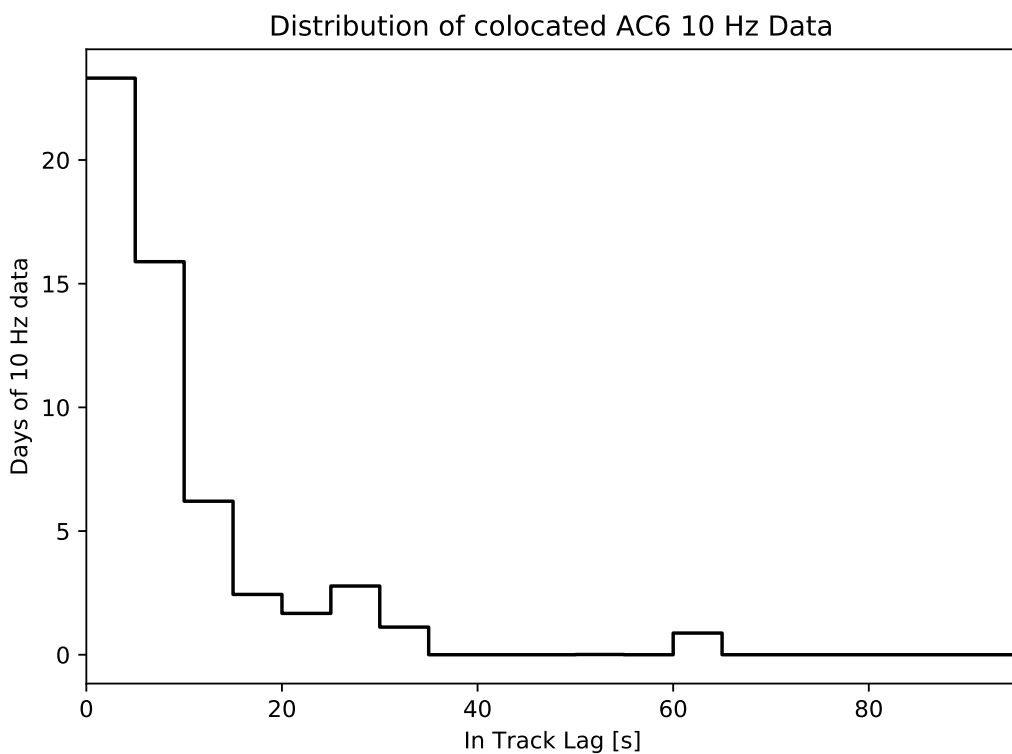


**Figure A1.** The distribution of colocated 10 Hz data as a function of in-track lag. Bins are 5 kilometers wide.

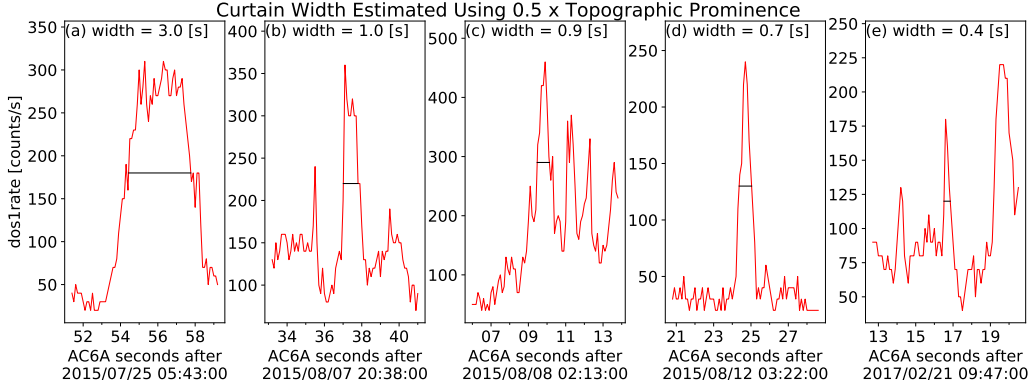


**Figure B1.** Five examples of curtains observed by AC6A shown with the red curves and the curtain widths are shown with the horizontal black lines. The height of the horizontal black lines are at half of the curtain's topographic prominence.

386 AC6-A in red (for clarity the AC6-B data is not shown), and the curtain width is shown  
387 by the horizontal black line.

### Acknowledgments

This work was made possible with the help from the many engineers and scientists at The Aerospace Corporation who designed, built, and operated AC6. M. Shumko was supported by NASA Headquarters under the NASA Earth and Space Science Fellowship Program - Grant 80NSSC18K1204 and NASA Postdoctoral Program at the NASA's Goddard Space Flight Center, administered by Universities Space Research Association under contract with NASA. D.L. Turner is thankful for funding from a NASA grant (prime award #: 80NSSC19K0280). The work at The Aerospace Corporation was supported in part by RBSP-ECT funding provided by JHU/APL contract 967399 under NASA's Prime contract NAS501072. The AC6 data and documentation is available at <http://rbspgway.jhuapl.edu/ac6> and the IRBEM-Lib version used for this analysis can be downloaded from <https://sourceforge.net/p/irbem/code/616/tree/>.

### References

- 401 Anderson, K. A., & Milton, D. W. (1964). Balloon observations of X rays in the  
402 auroral zone: 3. High time resolution studies. *Journal of Geophysical Re-*  
403 *search*, 69(21), 4457–4479. Retrieved from <http://dx.doi.org/10.1029/JZ069i021p04457> doi: 10.1029/JZ069i021p04457
- 405 Blake, J. B.,Looper, M. D., Baker, D. N., Nakamura, R., Klecker, B., & Hoves-  
406 tadt, D. (1996). New high temporal and spatial resolution measurements by  
407 sampex of the precipitation of relativistic electrons. *Advances in Space Re-*  
408 *search*, 18(8), 171 - 186. Retrieved from <http://www.sciencedirect.com/science/article/pii/0273117795009698> doi: [http://dx.doi.org/10.1016/0273-1177\(95\)00969-8](http://dx.doi.org/10.1016/0273-1177(95)00969-8)
- 411 Blake, J. B., & O'Brien, T. P. (2016). Observations of small-scale latitudinal struc-  
412 ture in energetic electron precipitation. *Journal of Geophysical Research: Space*  
413 *Physics*, 121(4), 3031–3035. Retrieved from <http://dx.doi.org/10.1002/2015JA021815> (2015JA021815) doi: 10.1002/2015JA021815
- 415 Blum, L., Li, X., & Denton, M. (2015). Rapid MeV electron precipitation as ob-  
416 served by SAMPEX/HILT during high-speed stream-driven storms. *Jour-*  
417 *nal of Geophysical Research: Space Physics*, 120(5), 3783–3794. Retrieved

- 418 from <http://dx.doi.org/10.1002/2014JA020633> (2014JA020633) doi:  
 419 10.1002/2014JA020633
- 420 Blum, L., Schiller, Q., Li, X., Millan, R., Halford, A., & Woodger, L. (2013). New  
 421 conjunctive cubesat and balloon measurements to quantify rapid energetic  
 422 electron precipitation. *Geophysical research letters*, 40(22), 5833–5837.
- 423 Boscher, D., Bourdarie, S., O'Brien, P., Guild, T., & Shumko, M. (2012). *Irbem-lib*  
 424 *library*.
- 425 Breneman, A., Crew, A., Sample, J., Klumpar, D., Johnson, A., Agapitov, O., ...  
 426 others (2017). Observations directly linking relativistic electron microbursts  
 427 to whistler mode chorus: Van allen probes and FIREBIRD II. *Geophysical  
 428 Research Letters*.
- 429 Brown, J., & Stone, E. (1972). High-energy electron spikes at high latitudes. *Journal  
 430 of Geophysical Research*, 77(19), 3384–3396.
- 431 Brown, R., Barcus, J., & Parsons, N. (1965, 6). Balloon observations of auroral zone  
 432 x rays in conjugate regions. 2. microbursts and pulsations. *Journal of Geophys-  
 433 ical Research (U.S.)*, 70. doi: 10.1029/JZ070i011p02599
- 434 Comess, M., Smith, D., Selesnick, R., Millan, R., & Sample, J. (2013). Duskside  
 435 relativistic electron precipitation as measured by sampex: A statistical sur-  
 436 vey. *Journal of Geophysical Research: Space Physics*, 118(8), 5050-5058.  
 437 Retrieved from <https://agupubs.onlinelibrary.wiley.com/doi/abs/10.1002/jgra.50481> doi: 10.1002/jgra.50481
- 438 Crew, A. B., Spence, H. E., Blake, J. B., Klumpar, D. M., Larsen, B. A., O'Brien,  
 439 T. P., ... Widholm, M. (2016). First multipoint in situ observations of elec-  
 440 tron microbursts: Initial results from the NSF FIREBIRD II mission. *Jour-  
 441 nal of Geophysical Research: Space Physics*, 121(6), 5272–5283. Retrieved  
 442 from <http://dx.doi.org/10.1002/2016JA022485> (2016JA022485) doi:  
 443 10.1002/2016JA022485
- 444 Dietrich, S., Rodger, C. J., Clilverd, M. A., Bortnik, J., & Raita, T. (2010). Rela-  
 445 tivistic microburst storm characteristics: Combined satellite and ground-based  
 446 observations. *Journal of Geophysical Research: Space Physics*, 115(A12).
- 447 Douma, E., Rodger, C., Blum, L., O'Brien, T., Clilverd, M., & Blake, J. (2019).  
 448 Characteristics of relativistic microburst intensity from sampex observations.  
 449 *Journal of Geophysical Research: Space Physics*.
- 450 Douma, E., Rodger, C. J., Blum, L. W., & Clilverd, M. A. (2017). Occurrence  
 451 characteristics of relativistic electron microbursts from SAMPEX observations.  
 452 *Journal of Geophysical Research: Space Physics*, 122(8), 8096–8107. Retrieved  
 453 from <http://dx.doi.org/10.1002/2017JA024067> (2017JA024067) doi:  
 454 10.1002/2017JA024067
- 455 Greeley, A., Kanekal, S., Baker, D., Klecker, B., & Schiller, Q. (2019). Quantifying  
 456 the contribution of microbursts to global electron loss in the radiation belts.  
 457 *Journal of Geophysical Research: Space Physics*.
- 458 Hoffman, R. A., & Evans, D. S. (1968). Field-aligned electron bursts at high lati-  
 459 tudes observed by ogo 4. *Journal of Geophysical Research*, 73(19), 6201–6214.
- 460 Imhof, W., Voss, H., Mobilia, J., Datlowe, D., & Gaines, E. (1991). The precipita-  
 461 tion of relativistic electrons near the trapping boundary. *Journal of Geophys-  
 462 ical Research: Space Physics*, 96(A4), 5619–5629.
- 463 Johnson, A., Shumko, M., Griffith, B., Klumpar, D., Sample, J., Springer, L., ...  
 464 others (2020). The FIREBIRD-II CubeSat mission: Focused investigations of  
 465 relativistic electron burst intensity, range, and dynamics. *Review of Scientific  
 466 Instruments*, 91(3), 034503.
- 467 Lehtinen, N. G., Inan, U. S., & Bell, T. F. (2000). Trapped energetic electron  
 468 curtains produced by thunderstorm driven relativistic runaway electrons. *Geo-  
 469 physical research letters*, 27(8), 1095–1098.
- 470 Lorentzen, K. R., Blake, J. B., Inan, U. S., & Bortnik, J. (2001). Observations of  
 471 relativistic electron microbursts in association with VLF chorus. *Journal of*

- Geophysical Research: Space Physics*, 106(A4), 6017–6027. Retrieved from <http://dx.doi.org/10.1029/2000JA003018> doi: 10.1029/2000JA003018

Lorentzen, K. R., Looper, M. D., & Blake, J. B. (2001). Relativistic electron microbursts during the GEM storms. *Geophysical Research Letters*, 28(13), 2573–2576. Retrieved from <http://dx.doi.org/10.1029/2001GL012926> doi: 10.1029/2001GL012926

Marklund, G. T., Sadeghi, S., Cumnock, J. A., Karlsson, T., Lindqvist, P.-A., Nilsson, H., ... others (2011). Evolution in space and time of the quasi-static acceleration potential of inverted-v aurora and its interaction with alfvénic boundary processes. *Journal of Geophysical Research: Space Physics*, 116(A1).

Millan, R., & Thorne, R. (2007). Review of radiation belt relativistic electron losses. *Journal of Atmospheric and Solar-Terrestrial Physics*, 69(3), 362 – 377. Retrieved from <http://www.sciencedirect.com/science/article/pii/S1364682606002768> doi: <http://dx.doi.org/10.1016/j.jastp.2006.06.019>

O'Brien, T. P., Blake, J. B., & W., G. J. (2016, May). *AeroCube-6 dosimeter data README* (Tech. Rep. No. TOR-2016-01155). The Aerospace Corporation.

O'Brien, T. P., Looper, M. D., & Blake, J. B. (2019, July). *AeroCube-6 dosimeter equivalent energy thresholds and flux conversion factors* (Tech. Rep. No. TOR-2017-02598). The Aerospace Corporation.

O'Brien, T. P., Lorentzen, K. R., Mann, I. R., Meredith, N. P., Blake, J. B., Fen nell, J. F., ... Anderson, R. R. (2003). Energization of relativistic electrons in the presence of ULF power and MeV microbursts: Evidence for dual ULF and VLF acceleration. *Journal of Geophysical Research: Space Physics*, 108(A8). Retrieved from <http://dx.doi.org/10.1029/2002JA009784> doi: 10.1029/2002JA009784

Olson, W. P., & Pfitzer, K. A. (1982). A dynamic model of the magnetospheric magnetic and electric fields for july 29, 1977. *Journal of Geophysical Research: Space Physics*, 87(A8), 5943–5948. Retrieved from <http://dx.doi.org/10.1029/JA087iA08p05943> doi: 10.1029/JA087iA08p05943

Parks, G. K. (1967). Spatial characteristics of auroral-zone X-ray microbursts. *Journal of Geophysical Research*, 72(1), 215–226.

Partamies, N., Donovan, E., & Knudsen, D. (2008). Statistical study of inverted-v structures in fast data. In *Annales geophysicae* (Vol. 26, pp. 1439–1449).

Randall, C. E., Harvey, V. L., Holt, L. A., Marsh, D. R., Kinnison, D., Funke, B., & Bernath, P. F. (2015). Simulation of energetic particle precipitation effects during the 2003–2004 arctic winter. *Journal of Geophysical Research: Space Physics*, 120(6), 5035–5048.

Selesnick, R. S., Blake, J. B., & Mewaldt, R. A. (2003). Atmospheric losses of radiation belt electrons. *Journal of Geophysical Research: Space Physics*, 108(A12). Retrieved from <http://dx.doi.org/10.1029/2003JA010160> (1468) doi: 10.1029/2003JA010160

Seppälä, A., Douma, E., Rodger, C., Verronen, P., Clilverd, M. A., & Bortnik, J. (2018). Relativistic electron microburst events: Modeling the atmospheric impact. *Geophysical Research Letters*, 45(2), 1141–1147.

Shumko, M., Johnson, A., Sample, J., Griffith, B. A., Turner, D. L., O'Brien, T. P., ... Claudepierre, S. G. (2020). Electron microburst size distribution derived with AeroCube-6. *Journal of Geophysical Research: Space Physics*, e2019JA027651.

Thieman, J. R., & Hoffman, R. A. (1985). Determination of inverted-v stability from dynamics explorer satellite data. *Journal of Geophysical Research: Space Physics*, 90(A4), 3511–3516.

Thorne, R. M., O'Brien, T. P., Shprits, Y. Y., Summers, D., & Horne, R. B. (2005). Timescale for MeV electron microburst loss during geomagnetic storms. *Journal of Geophysical Research: Space Physics*, 110(A9). Retrieved from <http://dx.doi.org/10.1029/2004JA010296> doi: 10.1029/2004JA010296

528                    [dx.doi.org/10.1029/2004JA010882](http://dx.doi.org/10.1029/2004JA010882) (A09202) doi: 10.1029/2004JA010882  
529        Tsygankenko, N. (1989). A solution of the chapman-ferraro problem for an el-  
530        lipsoidal magnetopause. *Planetary and Space Science*, 37(9), 1037 - 1046.  
531        Retrieved from <http://www.sciencedirect.com/science/article/pii/0032063389900767> doi: [http://dx.doi.org/10.1016/0032-0633\(89\)90076-7](http://dx.doi.org/10.1016/0032-0633(89)90076-7)  
532